

Microwave Surface Impedance and Complex Conductivity of High- T_c Single Crystals: Current State and Unsolved Problems

Yu. A. Nefyodov,¹ A. F. Shevchun,¹ A. M. Shuvaev,¹ and M. R. Trunin¹

Published online: 9 February 2007

Common and distinctive features of the temperature dependences of microwave surface impedance $Z(T) = R(T) + iX(T)$ and conductivity $\sigma(T)$ in the ab -plane and along the c -axis of high- T_c single crystals (HTSC) are discussed. The main attention is focused on an evolution of these dependences in YBaCuO crystal with the oxygen deficiency. Comparison of YBaCuO with other HTSC crystals reveals a number of peculiarities, namely, the linear dependence $R_{ab}(T) \propto T$ up to $T_c/2$ in HTSC single crystals with tetragonal lattice and up to $T_c/3$ in YBaCuO where $R_{ab}(T)$ shows also a broad peak at $T \sim T_c/2$; breakdown of normal skin effect in some HTSC crystals; dramatic effect of pseudogap on the superfluid density in the heavily underdoped YBCO; several orders of magnitude higher residual surface resistance in HTSC when compared to conventional superconductors; etc. Possible explanations are discussed in the context of the specific features of HTSC structure and in the framework of recent models of quasiparticles' c -transport and pseudogap state in HTSC.

KEY WORDS: high-temperature superconductors; surface impedance; microwave conductivity; anisotropy; pseudogap; single crystals.

1. INTRODUCTION

In past years, a lot of interest has been focused on investigations of transport properties evolution in high- T_c single crystals (HTSC) with different level of doping by oxygen and other substitutional impurities; in other words, the dependence upon the number p of holes per Cu atom in the CuO_2 plane. The p value and the critical temperature T_c of a superconducting transition in HTSC satisfy the following empirical relationship¹:

$$T_c = T_{c,\max}[1 - 82.6(p - 0.16)^2].$$

The narrow band of HTSC phase diagram corresponding to the optimal doping ($p \approx 0.16$) and maximum values of the critical temperature $T_c = T_{c,\max}$

is the most studied area. In the normal state of optimally doped HTSC, the resistivity $\rho_{ab}(T)$ of cuprate ab -planes increases proportionally to temperature viz., $\Delta\rho_{ab}(T) \propto T$. The resistivity $\rho_c(T)$ in perpendicular direction substantially exceeds the value of $\rho_{ab}(T)$ and also has metallic behavior (both $\rho_{ab}(T)$ and $\rho_c(T)$ increase with T). However, BiSrCaCuO, which is the most anisotropic HTSC (having $\rho_c/\rho_{ab} \approx 10^5$ at $p \approx 0.16$) represents an exception: its resistivity $\rho_c(T)$ increases as T approaches T_c ($d\rho_c(T)/dT < 0$). A measure of HTSC anisotropy in the superconducting state is the ratio $\sigma''_{ab}(0)/\sigma''_c(0) = \lambda_c^2(0)/\lambda_{ab}^2(0)$, where σ''_{ab} and σ''_c are imaginary parts of conductivity, λ_{ab} and λ_c are penetration depths of high-frequency field for currents running in the ab -planes and perpendicular to them, respectively. It is a common knowledge that $\Delta\lambda_{ab}(T) \propto T$ at $T < T_c/3$ in high-quality HTSC crystals and this experimental fact provides strong evidence for $d_{x^2-y^2}$ symmetry of the order parameter in these materials. However, there is no consensus in literature about $\Delta\lambda_c(T)$ behavior at

¹Institute of Solid State Physics, Russian Academy of Sciences, 142432 Chernogolovka, Moscow, Russia; e-mail: nefyodov@issp.ac.ru.

low temperatures. Even $\text{YBa}_2\text{Cu}_3\text{O}_{6.95}$ ($T_c \approx 93$ K), the most thoroughly studied single crystals have shown both linear ($\Delta\lambda_c(T) \propto T$) [2–4], and quadratic dependences⁵ in the range $T < T_c/3$.

Pseudogap states appearing at $p < 0.16$ occupy a wide band of HTSC phase diagram, which is far less investigated. Measurements of *ac*-susceptibility of oriented HTSC powders at $T < T_c$ show⁶ that their $\sigma_c''(T)/\sigma_c''(0)$ dependences have smaller slope at $T \rightarrow 0$ than $\sigma_{ab}''(T)/\sigma_{ab}''(0)$ dependences. The normal state of underdoped HTSC is characterized by nonmetallic behavior of the resistivity $\rho_c(T)$ at T approaching T_c , by deviation of the *ab*-plane resistivity from its linear dependence $\Delta\rho_{ab}(T) \propto T$ and by ρ_c/ρ_{ab} ratio rising dramatically with the decrease of p . A lot of theoretical models have been proposed to explain these properties, but there are none fully describing the evolution of the dependences $\sigma_{ab}''(T)$, $\sigma_c''(T)$ and $\rho_{ab}(T)$, $\rho_c(T)$ in the wide range of concentration p and temperature T .

Among the experimental methods of studying these problems, there are the measurements of the temperature dependences of the surface impedance $Z(T) = R(T) + iX(T)$. In the local electrodynamics, which applies to HTSC, $Z(T)$ defines the complex conductivity tensor $\hat{\sigma}(T) = \hat{\sigma}'(T) - i\hat{\sigma}''(T) = i\omega\mu_0/Z^2(T)$ characterized by the components σ_{ab} and σ_c . At microwave frequencies, the imaginary part of the surface impedance—the surface reactance X —reflects mainly the response of the superconducting carries. The real part—the surface resistance R —is proportional to the microwave losses and is due to the normal carriers.

In the present paper, we will analyze the common and distinctive features of $Z(T)$ and $\hat{\sigma}(T)$ curves in HTSC single crystals. Our main attention in this analysis will be focused on the evolution of these curves in $\text{YBa}_2\text{Cu}_3\text{O}_{7-x}$ crystal with the oxygen deficiency varied in the range $0.07 \leq x \leq 0.47$.

2. EXPERIMENT

The experiments were performed by the “hot-finger” technique⁷ at the frequency of $\omega/2\pi = 9.4$ GHz and in the temperature range $5 \leq T \leq 200$ K. The initial $\text{YBa}_2\text{Cu}_3\text{O}_{6.93}$ crystal was grown in BaZrO_3 crucible and had a rectangular shape with dimensions being $1.6 \text{ mm} \times 0.4 \text{ mm} \times 0.1 \text{ mm}$. To change the carrier density, we successively annealed the crystal in the air at various temperatures $T \geq 500^\circ\text{C}$ and quenched it with liquid nitrogen. Finally, five crystal states with critical temperatures $T_c = 92, 80, 70, 57, 41$ K and, correspondingly, the concentrations $p = 0.16, 0.12, 0.106, 0.092, 0.078$ were investigated (Table I). Anisotropy was measured for each of the five states. The whole cycle of the microwave anisotropy measurements includes the following⁴: (i) we measure the temperature dependences of the quality factor and of the frequency shift of the superconducting niobium resonator with the sample inside in the two crystal orientations with respect to the microwave magnetic field, namely, transversal (T) and longitudinal (L); (ii) measurements in the T -orientation gave the surface resistance $R_{ab}(T)$, reactance $X_{ab}(T)$ and conductivity $\sigma_{ab}(T) = i\omega\mu_0/Z_{ab}^2(T)$ of the crystal cuprate planes, both in the normal and superconducting states; and (iii) measurements in the L -orientation gave $\sigma_c(T)$, $X_c(T)$, $R_c(T)$.

3. NORMAL STATE

The temperature dependences of surface impedance components in the *ab*-plane, $R_{ab}(T)$ and $X_{ab}(T)$, and along *c*-axis, $R_c(T)$ and $X_c(T)$ are shown in Fig. 1 for each of the five crystal states indicated in Table I. The $X_{ab}(T)$ dependences in Fig. 1(a) are constructed with allowance made for both (i) the

Table I. Annealing and Critical Temperatures, Doping Parameters, Characteristics of the Microwave *ab*-plane Response [Transition Width δT_c , Residual Surface Resistance R_{res} , Relaxation Time $\tau_{ab}(T_c)$, Parameter $\beta \approx \tau_{ab}(T_c)/\tau_{ab}(0)$] and Penetration Depths in $\text{YBa}_2\text{Cu}_3\text{O}_{7-x}$ Crystal

Annealing temperature T ($^\circ\text{C}$)	Critical temperature T_c (K)	Doping parameters		<i>ab</i> -Plane characteristics				λ values at $T = 0$		$\Delta\lambda_c(T) \propto T^\alpha$ α	λ_c/λ_{ab} at $T = 0$
		p	x	δT_c (K)	R_{res} ($\mu\Omega$)	$\tau_{ab}(T_c) \times 10^{13}$ (s)	β	λ_{ab} (nm)	λ_c (μm)		
500	92	0.16	0.07	0.5	55	0.7	0.05	152	1.55	1.0	10
520	80	0.12	0.26	1	54	0.9	0.06	170	3.0	1.1	18
550	70	0.106	0.33	1.5	50	1.0	0.10	178	5.2	1.2	29
600	57	0.092	0.40	1.5	35	1.4	0.13	190	6.9	1.3	36
720	41	0.078	0.47	4.0	30	1.5	0.20	198	16.3	1.8	83

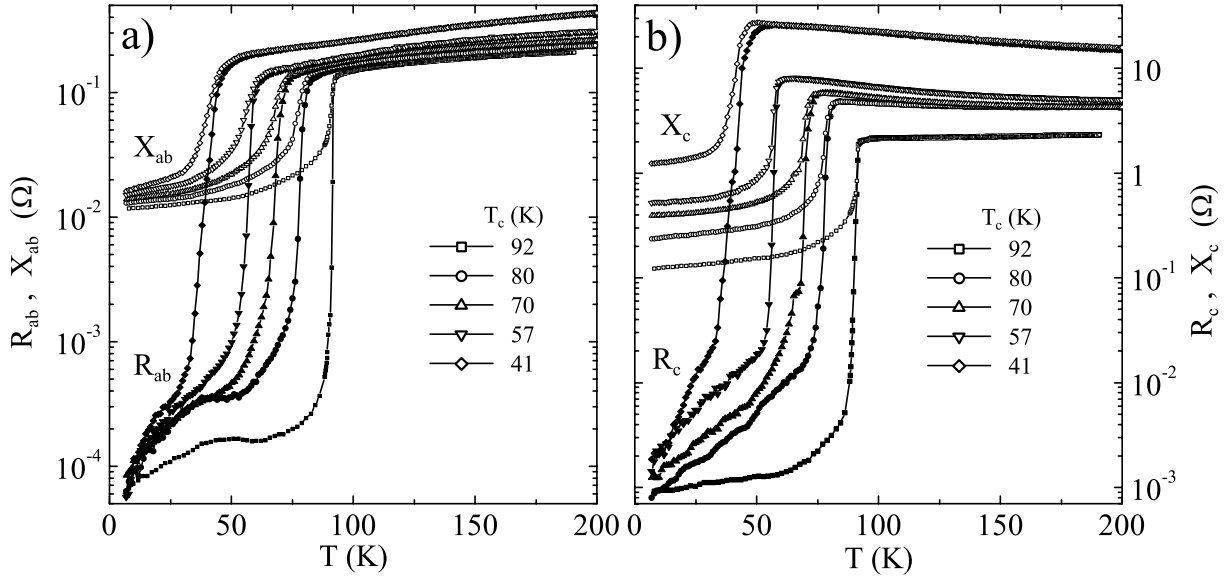


Fig. 1. (a) real $R_{ab}(T)$ (solid symbols) and imaginary $X_{ab}(T)$ (open symbols) parts of the ab -plane surface impedance of the five states of $\text{YBa}_2\text{Cu}_3\text{O}_{7-x}$ single crystal; (b) the components of the c -axis surface impedance.

contribution $\Delta X_{ab}^{\text{th}}(T)$ of thermal expansion of the crystal, which essentially affects the measured reactance shift $\Delta X_{ab}(T)$ at $T > 0.9 T_c$, and (ii) the additive constant X_0 , which is equal to the difference between the values of $[\Delta X_{ab}(T) + \Delta X_{ab}^{\text{th}}(T)]$ and $R_{ab}(T)$ at $T > T_c$: $X_{ab}(T) = \Delta X_{ab}(T) + \Delta X_{ab}^{\text{th}}(T) + X_0$. The detailed procedure of the $Z_c(T)$ determination from the quantities measured is described in ⁴.

In the normal state, we have $R_{ab}(T) = X_{ab}(T)$ and $R_c(T) = X_c(T)$, which implies the validity of the normal skin-effect condition. Therefore, the resistivities $\rho_{ab}(T)$ and $\rho_c(T)$ can be found from $R_{ab}(T)$ and $R_c(T)$ curves at $T > T_c$, as shown in Fig. 1, applying the standard formulas of the normal skin effect: $\rho_{ab}(T) = 2R_{ab}^2(T)/\omega\mu_0$, $\rho_c(T) = 2R_c^2(T)/\omega\mu_0$. Figure 2 shows the evolution of the dependences $\rho_{ab}(T)$ and $\rho_c(T)$ in the temperature range $T_c < T \leq 200$ K for $\text{YBa}_2\text{Cu}_3\text{O}_{7-x}$ crystal with the change of x . Only the optimally doped $\text{YBa}_2\text{Cu}_3\text{O}_{6.93}$ shows that both dependences $\rho_{ab}(T)$ and $\rho_c(T)$ have a metallic behavior, and the ratio ρ_c/ρ_{ab} approaches the anisotropy of the effective mass of charge carriers $m_c/m_{ab} = \lambda_c^2(0)/\lambda_{ab}^2(0)$ in the pure three-dimensional (3D) London superconductor of the type $\text{YBa}_2\text{Cu}_3\text{O}_{6.93}$. The other states of $\text{YBa}_2\text{Cu}_3\text{O}_{7-x}$ with lower concentration of holes have the resistivity $\rho_c(T)$ increasing with the decrease of temperature, which shows its nonmetallic

behavior. A crossover from Drude conductivity (at $x = 0.07$) along the c -axis to the tunneling one (at $x > 0.07$) takes place. This is proved in ⁸ by both estimating minimum metallic c -conductivity and maximum tunneling c -conductivity and quantitatively comparing the measured dependences $\rho_c(T)$ with the ones calculated in the polaron model of quasiparticles' c -transport⁹. According to this model, the interplanar tunneling of quasiparticles is considered as a perturbation of a strongly coupled electron-phonon system. In the c -direction, an electron is surrounded by a large number of phonons, forming a polaron¹⁰, which influences the transversal ab -transport weakly. The following analytic expression was obtained in ⁹ for Einsteinian spectrum of c -polarized phonons in the temperature range $T \sim \omega_0$:

$$\rho_c(T) \propto \rho_{ab}(T) \frac{\exp[g^2 \tanh(\omega_0/4T)]}{\sqrt{\sinh(\omega_0/2T)}}, \quad (1)$$

where ω_0 is a typical phonon energy, g is a parameter characterizing strength of electron-phonon interaction and $g > 1$. Figure 3 represents our result of comparing experimental dependences $\rho_c(T)$ (symbols) and those calculated from Eq. (1) (solid lines). To calculate them, we used $\rho_{ab}(T)$ data in Fig. 2; g was almost the same for all the dependences in Fig. 3: $g \approx 3$; ω_0 increased from 110 K (75 cm^{-1}) to 310 K

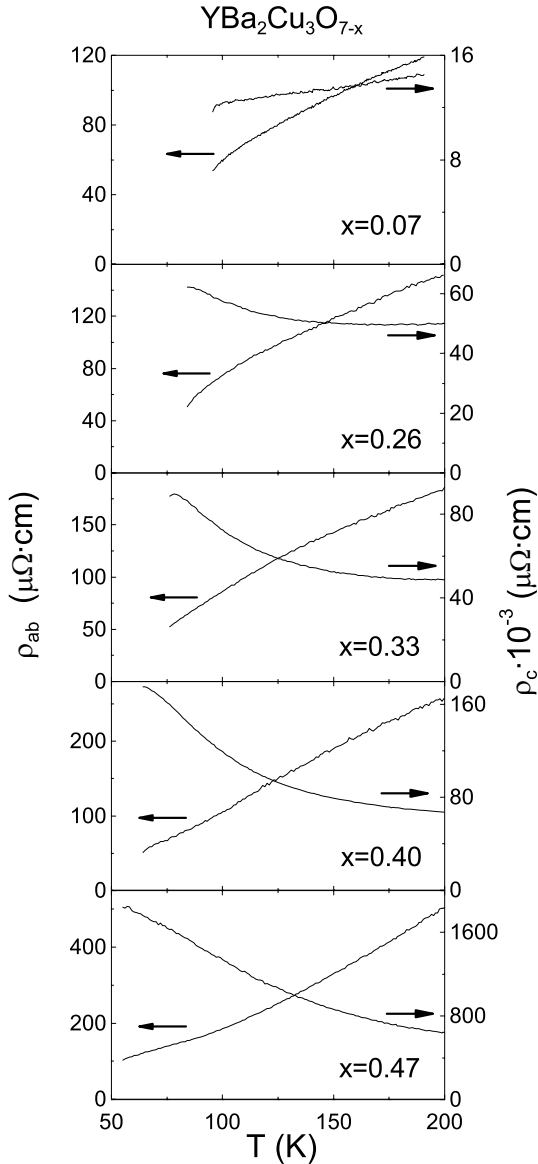


Fig. 2. The evolution of the measured $\rho_{ab}(T)$ and $\rho_c(T)$ dependences in $\text{YBa}_2\text{Cu}_3\text{O}_{7-x}$ with different oxygen content.

(215 cm^{-1}) when the oxygen content ($7-x$) was decreased in $\text{YBa}_2\text{Cu}_3\text{O}_{7-x}$ from 6.93 to 6.53.

At the same time, the ab -plane transport in the normal state of $\text{YBa}_2\text{Cu}_3\text{O}_{7-x}$ crystal always remains metallic. The value of $\rho_{ab}(T) \leq 50\ \mu\Omega\cdot\text{cm}$ is indicative of high quality of the crystal. As in the normal metals, in the ab -planes of optimally doped HTSC, the resistivity increases proportionally to temperature, $\Delta\rho_{ab}(T) \propto 1/\tau_{ab}(T) \propto T$, where τ_{ab} is a quasiparticle relaxation time in the cuprate planes.

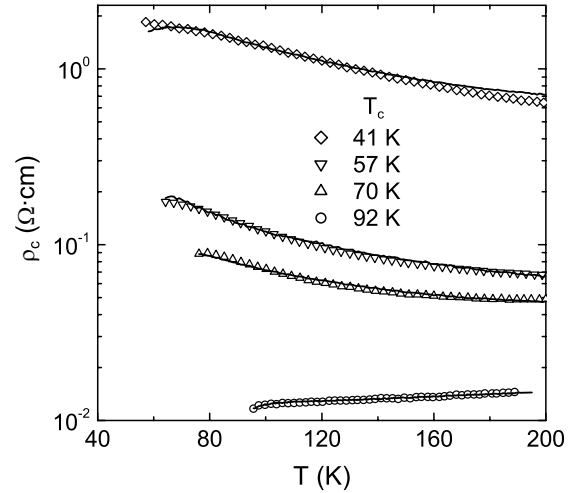


Fig. 3. Comparison of the experimental dependences $\rho_c(T)$ in $\text{YBa}_2\text{Cu}_3\text{O}_{7-x}$ (symbols) and those calculated from Eq. (1) (solid lines).

Assuming that scattering processes in this liquid are similar to those in metals, in ¹¹ we proposed the Bloch–Grüneisen formula (electron–phonon interaction) for the function $\tau_{ab}(T)$ in the normal and superconducting states of HTSC and retained the temperature-independent impurity relaxation time $\tau_{ab}(0)$, which is present in the Gorter and Casimir two-fluid model:

$$\frac{1}{\tau_{ab}(t)} = \frac{1}{\tau_{ab}(0)} \left[1 + \frac{t^5 \mathcal{J}_5(\kappa/t)/\mathcal{J}_5(\kappa)}{\beta} \right], \quad (2)$$

$$\mathcal{J}_5(\kappa/t) = \int_0^{\kappa/t} \frac{z^5 e^z dz}{(e^z - 1)^2},$$

where $t \equiv T/T_c$, $\kappa = \Theta/T_c$ (Θ is the Debye temperature) and β is a numerical parameter, which equals (as it follows from Eq. (2)) $\beta = \tau_{ab1}(T_c)/[\tau_{ab}(0) - \tau_{ab}(T_c)]$. Following the formal analogy with metals, one can say that the parameter β is the characteristic of the “HTSC purity”: $\beta \approx \tau_{ab}(T_c)/\tau_{ab}(0) \ll 1$ if $\tau_{ab}(0) \gg \tau_{ab}(T_c)$. The parameter Θ in HTSC can be estimated at several hundred degrees. At $T < \Theta/10$ ($\kappa > 10t$), the second summand in the square brackets in Eq. (2) is proportional to T^5 ; in the region $T > \Theta/5$ ($\kappa < 5t$), it is proportional to T . Thus, the reciprocal relaxation time is almost constant and equal to $1/\tau_{ab}(0)$ over the interval $0 < T < T_c/3$, and at higher temperatures it increases gradually, starting as the power function $\propto T^5$ in the region $T < T_c/2$ and changing later to function $\propto T$ around T_c ; at $T > T_c$ we have linear dependence $\Delta\rho_{ab}(T) \propto 1/\tau_{ab}(T) \propto T$.

Whereas the conditions $R_{ab}(T) = X_{ab}(T)$ at $T \geq T_c$ and $\Delta X_{ab}(T) < \Delta R_{ab}(T)$ at $T \lesssim T_c$ were experimentally proved for YBaCuO [12–17], BiSrCaCuO [12,15,17–19], TlBaCaCuO¹⁷, LaSrCuO²⁰, and BaKBiO¹¹ in the crystals of TlBaCuO^{21,22}, HgBaCuO, and HgBaCaCuO²² the reactance variation $\Delta X_{ab}(T)$ is considerably larger than that of the resistance $\Delta R_{ab}(T)$ in the entire temperature range such that $R_{ab}(T) \neq X_{ab}(T)$ at $T \gtrsim T_c$. In ²², this breakdown of the normal skin-effect condition was treated in terms of a collective phason mode. In model²³, the appearance of the strong inequality $R_{ab}(T) \neq X_{ab}(T)$ was due to the presence of superconducting islands embedded in a normal metallic matrix. Both concepts are related to the pseudogap phenomenon in HTSC. As an alternative explanation, we propose to allow for the shielding effect of the microwave field by roughnesses (cleavage plane traces), which may crop out at TlBaCuO crystal surface. If the penetration depth is much less than roughness sizes, both components of the effective surface impedance, that are measured will increase in comparison with their values for a flat surface by the same factor equal to the ratio of the real and flat surface areas. If the roughness sizes are comparable to the penetration depth the situation may occur when the microwave magnetic field \mathbf{H}_ω is slightly distorted by the roughness, whereas the high-frequency current \mathbf{j}_ω caused by the field decays noticeably²⁴. In this case, the effective reactance ($\sim \omega\mu_0 \int H_\omega^2 dV$) will exceed the sample surface resistance ($\sim \int \mathbf{j}_\omega^* E_\omega dV$). It is likely that this is the case for TlBaCuO crystal whose roughness' dimensions proved to be comparable with its skin depth. Indeed, scanning electron micrographs demonstrated²⁵ that the traces of the cleavage planes form juts (grooves) in the form of parallel channels at the surface of TlBaCuO crystal and the sizes (height, width, spacing) of these roughnesses are about of 1–2 μm .

4. SUPERCONDUCTING STATE

Figure 4 shows the low-temperature sections of the measured $\lambda_{ab}(T) = X_{ab}(T)/\omega\mu_0$ curves for five states of YBa₂Cu₃O_{7-x} crystal. The error in the absolute value of $\lambda_{ab}(T)$ is mainly caused by the accuracy of the additive constant X_0 determination. In our experiments the root-mean-square difference between $R_{ab}(T)$ and $X_{ab}(T)$ in the normal state corresponded to about 5 nm accuracy in $\lambda_{ab}(T)$ value.

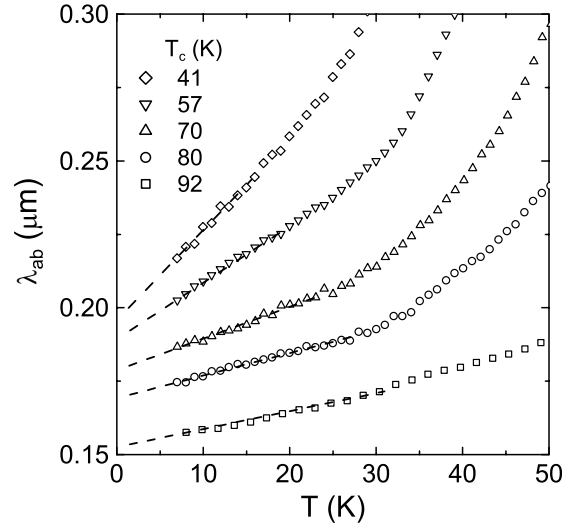


Fig. 4. Low-temperature dependences of $\lambda_{ab}(T)$ (open symbols) measured for five states of YBa₂Cu₃O_{7-x} crystal with $T_c = 92$ K, $T_c = 80$ K, $T_c = 70$ K, and $T_c = 41$ K. Dashed lines are linear extrapolations at $T < T_c/3$.

In YBa₂Cu₃O_{6.93} ($p = 0.16$), the temperature dependence $R_{ab}(T)$ has a broad peak in the range $T \sim T_c/2$, which is the characteristic for high-quality optimally doped YBaCuO crystals. The peak gradually vanishes with decreasing value of p . Note that such a peak has not been observed in any crystals with tetragonal (BiSrCaCuO, TlBaCaCuO, TlBaCuO, LaSrCuO) or cubic (BaKBiO) lattices.

The conductivity components $\sigma'(T)$ and $\sigma''(T)$ are not measured directly, but can be derived from measurements of $R(T)$ and $X(T)$:

$$\sigma' = \frac{2\omega\mu_0 R X}{(R^2 + X^2)^2}, \quad \sigma'' = \frac{\omega\mu_0 (X^2 - R^2)}{(R^2 + X^2)^2}. \quad (3)$$

At temperatures not very close to T_c , $R(T) \ll X(T)$ in HTSC (Fig. 1) and, hence, $\sigma''(T)$ curve is determined by the function $X(T) = \omega\mu_0 \lambda(T)$ alone and reflects the properties of the magnetic field penetration depth. The shape of $\sigma'(T)$ curve depends on the value of the residual surface resistance $R_{\text{res}} = R(T \rightarrow 0)$, which is obtained by the extrapolation of $R(T)$ curve to zero temperature in the region $T < T_c/3$. It follows from Eq. (3) that $\sigma'(T)$ curve has a peak at $T < T_c$ if the value of R_{res} is sufficiently small²⁶:

$$R_{\text{res}} < \frac{X(0)}{3} \left. \frac{dR(T)}{dX(T)} \right|_{T \rightarrow 0}. \quad (4)$$

This peak shifts to lower temperatures as R_{res} increases, and when the inequality Eq. (4) is violated, it

completely disappears. Figure 5 shows $\sigma'_{ab}(T)$ curves for five states of $\text{YBa}_2\text{Cu}_3\text{O}_{7-x}$ with different oxygen content (Table I). Usually $\sigma'(T)$ in HTSC single crystals has also a narrow peak near T_c (Fig. 5). Its width equals the width of the superconducting transition on the curve of $R(T)$ at microwave frequencies.

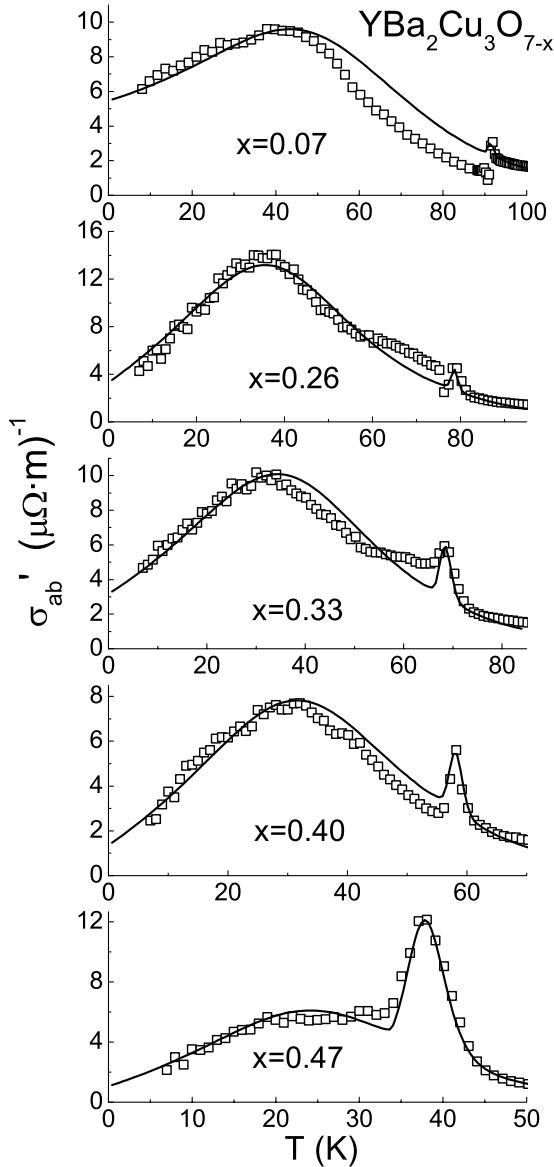


Fig. 5. The conductivities $\sigma'_{ab}(T)$ (symbols) of the five states of $\text{YBa}_2\text{Cu}_3\text{O}_{7-x}$ crystal extracted from the surface impedance measurements of Fig. 1(a) and the calculations (solid lines) based on the modified two-fluid model, which takes into account the inhomogeneous broadening δT_c of the superconducting transition and residual surface resistance R_{res} (Table I).

Even though the form chosen for the function $\tau_{ab}(T)$ in Eq. (2) is oversimplified in the case of HTSC materials with complex electronic spectra, it is turned out that all common and even specific features of $R_{ab}(T)$ and $\sigma'_{ab}(T)$ curves for both $T < T_c$ and $T > T_c$ are adequately described by the modified two-fluid model (MTFM) with the only free-fitting parameter κ in Eq. (2).

Indeed, in the case of $(\omega\tau_{ab})^2 \ll 1$, which is typical for HTSC crystals at all temperatures in the frequency band around 10 GHz or below, the components of the complex conductivity $\sigma = \sigma' - i\sigma''$ can be written in a very simple form:

$$\sigma' = \frac{n_n e^2 \tau_{ab}}{m}, \quad \sigma'' = \frac{n_s e^2}{m\omega}, \quad (5)$$

where $n_{n,s}(T)$ are the densities of the normal and superconducting carriers (both having the same charge e and effective mass m). At temperatures $T \leq T_c$, the total carrier concentration $n = n_s + n_n$ is equal to the concentration of quasiparticles in the normal state. From the values of $R_{ab}(T_c)$ and $X_{ab}(0)$, and the slopes dR_{ab}/dT and dX_{ab}/dT at $T \ll T_c$, one can easily derive the parameters²⁶

$$\omega\tau_{ab}(T_c) = \frac{X_{ab}^2(0)}{2R_{ab}^2(T_c)}, \quad \omega\tau_{ab}(0) = \left. \frac{dR_{ab}}{dX_{ab}} \right|_{T \rightarrow 0} \quad (6)$$

and determine the parameters β in Eq. (2), as indicated in Table I. Now, if we use the dependence $n_s(T)/n = \sigma''(T)/\sigma''(0) = \lambda^2(0)/\lambda^2(T)$ determined in the same experiment and, thus, derive the function $n_n(T)/n = 1 - n_s(T)/n$, we can fit the measurements of $R_{ab}(T)$ using Eqs. (2), (5) and free parameter κ by the general formula $R = \text{Re}[\sqrt{i\omega\mu_0}/(\sigma' - i\sigma'')]$. Then, we derive the real part of the conductivity $\sigma'_{ab}(T)$ using Eq. (3). Figure 5 shows the comparison of the experimental data with the calculations by the procedure given above. In addition, we took account of the inhomogeneous broadening δT_c of the superconducting transition (Table I) following the approach²⁶ that describes the peak in the conductivity $\sigma'(T)$ at a temperature $T_m = T_c - \delta T_c$, which is close to the critical temperature. The narrower the superconducting transition (the smaller δT_c), the smaller the peak amplitude. Furthermore, when comparing the calculations with the measurements of the surface resistance, we added to the functions $R(T)$, determined by the given above general formula, the values R_{res} from Table I. For this reason, the curves of $\sigma'_{ab}(T)$ in Fig. 5, which were calculated by Eq. (3), do not tend to zero as $T \rightarrow 0$, even though the carrier density $n_n = 0$ at $T = 0$, according to MTFM, and as it

follows from Eq. (5), the conductivity should tend to $\sigma(0) = 0$.

The origin of the residual losses in HTSC materials has remained unclear. In some works [27], these losses were attributed to the presence of a fraction n_0 of carriers that remain unpaired at $T = 0$. The magnitude of R_{res} was estimated by formula $R = \omega^2 \mu_0^2 \sigma' \lambda^3 / 2$, following from the general one at $T < T_c$, with the nonzero conductivity $\sigma'(0) = n_0 e^2 \tau_{ab}(0) / m$ from Eq. (5). One can easily prove, however, that this approach requires inequality Eq. (4) to be satisfied. If this condition is not met, which may occur in HTSC crystals^{17,26}, the number n_0 needed to describe R_{res} value will be larger than the entire concentration n of the carriers.

In developing the traditional approach to the problem, which attributed the residual surface resistance to various imperfections of the surface, the researchers took account of the losses due to weak links [28–30], twinning planes^{30,31}, clusters with normal conductivity³², etc. Numerical estimates, however, indicate that the contribution of these mechanisms to the residual surface resistance is much smaller than R_{res} measured in HTSC materials. Moreover, a very remarkable fact is that the residual surface resistance measured at a frequency of 10 GHz was approximately the same, $R_{\text{res}} \sim 100 \mu\Omega$, in the ab -plane of all high-quality copper-oxide HTSC crystals of different chemical compositions and grown by different methods, irrespective of whether the samples contained twinning planes or not, and whether measurements were performed on freshly cleaved or as-grown surfaces. This fact, apparently, indicates that the presence of residual losses is the inherent feature of all HTSC which originates from their structure, namely, from their conspicuously layered nature. In other words, a fraction of current flowing in the surface layer of an HTSC crystal may run through regions of the layer that are in the normal state and have a finite resistivity ρ_n . In the phenomenological model under consideration, this contribution to the impedance can be included as a circuit element ρ_n connected in parallel to the two-fluid circuit characterized by Eq. (5), i.e., a resistor $\rho = 1/\sigma'$ shunted by a kinetic inductor $l = 1/\omega\sigma''$ (the parallel connection of ρ and l is in conformity with the formula relating the current to the field in the two-fluid model). Obviously, the complex impedance of the circuit consists of the imaginary part $iX = i\omega\mu_0\lambda$ at $T < T_c$ and the sum of two real components: the ordinary $R = \omega^2 \mu_0^2 \lambda^3 / 2\rho$ and $R_0 = \omega^2 \mu_0^2 \lambda^3 / 2\rho_n$. At $T = 0$, when $R(0) = 0$, only R_0 value defines the resid-

ual resistance R_{res} . At a frequency of 10 GHz, and using $R_{\text{res}} \approx 100 \mu\Omega$ and $\lambda(0) \approx 0.2 \mu\text{m}$ as an estimate, which are typical parameters for the ab -plane of HTSC crystals, we obtain $\rho_n(0) \approx 25 \mu\Omega \cdot \text{cm}$, that is quite usual value for normal metals.

To sum up this section, one can describe characteristic features of $R_{ab}(T)$ and $\sigma'_{ab}(T)$ curves in HTSC crystals by generalizing the well-known Gorter and Casimir two-fluid model. For this, we introduce a temperature dependence of quasiparticles relaxation time according to the Bloch–Grüneisen law. We conclude that $\sigma'_{ab}(T)$ curves can be well described by MTFM with the use of the only one free-fitting parameter, namely, $\kappa = \Theta/T_c$, while the other parameter $\beta = \tau_{ab}(T_c)/\tau_{ab}(0) \ll 1$ can be estimated directly from the experimental data with the aid of Eq. (6). The $\sigma'_{ab}(t)$ curve passes through a maximum at $t \lesssim 0.5$ if the inequality Eq. (4) is valid. This peak is due to the competition of two effects, namely, the decrease of normal carriers density as the temperature decreases and the increase of the relaxation time, which saturates at $t \sim \beta^{1/5}$, where the impurity scattering starts to dominate. From MTFM, it also follows that the absence of the broad peak of $R_{ab}(t)$ at $t \sim 0.5$ in $\text{YBa}_2\text{Cu}_3\text{O}_{7-x}$ with oxygen deficiency and in high-quality tetragonal HTSC single crystals is due to a less rapid increase of $\tau_{ab}(T)$ with decreasing temperature. In other words, the value of β is the smallest for the case of optimally doped YBaCuO crystals.

5. EFFECT OF PSEUDOGAP

Currently, the origin of the pseudogap remains unclear. Proposed theoretical scenarios can be divided into two categories. One is based on the idea that the pseudogap is due to precursor superconductivity, in which pairing takes place at the pseudogap transition temperature $T^* > T_c$ but achieves coherence only at T_c . The other assumes that the pseudogap state is not related to superconductivity per se, but rather competes with it. This magnetic precursor scenario of the pseudogap assumes dynamical fluctuations of some kind, such as spin, charge, structural, or so-called staggered flux phase. These two scenarios treat anomalies of electronic properties in underdoped HTSC observed at temperatures both above T_c and in its vicinity [33–36].

In the heavily underdoped HTSC, at $T \ll T_c$, a competition of pseudogap and superconducting order parameters develops most effectively and results

in the peculiarities of the superfluid density $n_s(T, p)$ as a function of temperature T and concentration p .

In a clean Bardeen, Cooper, and Schrieffer (BCS) d -wave superconductor (DSC) the dependence $\Delta n_s(T) \equiv n_s(T) - n_0$ is linear on temperature $T \ll T_c$: $\Delta n_s(T) \propto (-T/\Delta_0)$, where $n_0 = n_s(0)$ and $\Delta_0 = \Delta(0)$ are the superfluid density and the superconducting gap amplitude at $T = 0$. This dependence is confirmed by the measurements of the ab -plane penetration depth $\lambda_{ab}(T) = \sqrt{m^*/\mu_0 e^2 n_s(T)}$ in the optimally doped ($p = 0.16$) HTSC single crystals: $\Delta \lambda_{ab}(T) \propto T$ at $T < T_c/3$. The derivative $|dn_s(T)/dT|$ at $T \rightarrow 0$ determines n_0/Δ_0 ratio. If thermally excited fermionic quasiparticles are the only important excitations even at $p < 0.16$, then the slope of $n_s(T)$ curves at $T \ll T_c$ is proportional to $n_0(p)/\Delta_0(p)$ ratio: $|dn_s(T)/dT|_{T \rightarrow 0} \propto n_0(p)/\Delta_0(p)$.

In Fig. 4, the linear extrapolation (dashed lines) of the $\lambda_{ab}(T)$ dependences at $T < T_c/3$ gives the following $\lambda_{ab}(0)$ values³⁷: 152, 170, 178, 190, 198 nm for $p = 0.16, 0.12, 0.106, 0.092, 0.078$, respectively (Table I). As follows from Fig. 6, halving of the concentration (namely, from $p = 0.16$ to $p = 0.078$) results in approximately two times decrease of $\lambda_{ab}^{-2}(0)$ value. Similar behavior $n_0(p) \propto p$ within the range $0.08 < p \leq 0.16$ was observed by other groups^{38,39}. It is easily seen that this dependence contradicts Uemura's relation $n_0(p) \propto T_c(p)$ ⁴⁰. To the best of our knowledge, there are no data on the superfluid density in HTSC at $p < 0.08$. As for theoretical predictions, n_0 linearity on p extends down to $p = 0$ in the generalized Fermi-liquid models [41–43], while in the magnetic precursor d -density wave (DDW) scenario of pseudogap [44–46] it exists in the underdoped range of the phase diagram where the DSC order parameter grows from zero to its maximal value, moreover, $n_0(p)$ is nonzero as $\Delta_0(p)$ vanishes (Fig. 1 from⁴⁶). The latter agrees with our data.

In Fig. 6 we also show the slopes $|d\lambda_{ab}^{-2}(T)/dT|_{T \rightarrow 0} \propto |dn_s(T)/dT|_{T \rightarrow 0}$ of $\lambda_{ab}^{-2}(T)$ curves obtained from $\lambda_{ab}(T)$ dependences at $T < T_c/3$ in Fig. 4. The value of $|d\lambda_{ab}^{-2}(T)/dT|$ changes slightly at $0.1 < p \leq 0.16$ in accordance with model⁴¹, and measurements of YBa₂Cu₃O_{7-x} single crystals⁴⁷ and oriented powders⁴⁸ with the holes concentration $p \gtrsim 0.1$. However, it grows drastically at $p \lesssim 0.1$, namely, $\lambda_{ab}^{-2}(T)$ slope increases 2.5 times with the decrease of p from 0.12 to 0.08. The $|d\lambda_{ab}^{-2}(T)/dT| \propto p^{-2}$ dependence⁴² is shown by solid line in Fig. 6 and roughly fits the data at $p \leq 0.12$. The dotted line drawn through $|d\lambda_{ab}^{-2}(T)/dT|$ exper-

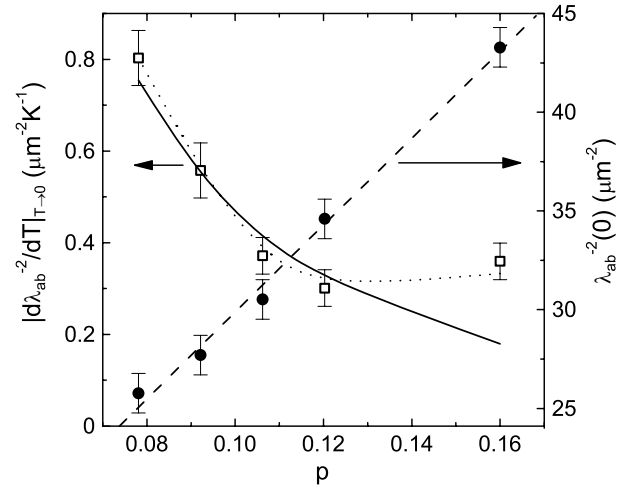


Fig. 6. The values of $\lambda_{ab}^{-2}(0) = n_s(0)\mu_0 e^2/m^*$ (right scale) and slopes $|d\lambda_{ab}^{-2}(T)/dT|_{T \rightarrow 0} = \mu_0 e^2/m^* |dn_s(T)/dT|_{T \rightarrow 0}$ (left scale) as a function of doping $p = 0.16 - \sqrt{(1 - T_c/T_{c,\max})}/82.6$ with $T_{c,\max} = 92$ K in YBa₂Cu₃O_{7-x}. Error bars correspond to experimental accuracy. The *dashed* and *dotted* lines guide the eye. The solid line is $|dn_s(T)/dT| \propto p^{-2}$ dependence.

imental points in Fig. 6 qualitatively agrees with the behavior of this quantity in the DDW model^{45,46}.

The temperature dependence of the superfluid density $n_s(T)$ at low T in the heavily underdoped YBa₂Cu₃O_{7-x} proves to be one more check-up of the DDW scenario of pseudogap. Also, $\lambda_{ab}^2(0)/\lambda_{ab}^2(T) = n_s(T)/n_0$ dependences obtained from the data in Fig. 4 are shown in Fig. 7(a) for different p values. The solid line represents the DSC result. The evident peculiarities in Fig. 7(a) are the concavity of $n_s(T)/n_0$ curves corresponding to the heavily underdoped states ($p = 0.078$ and $p = 0.092$) and their deviation from DSC and the curves for $p = 0.16, 0.12, 0.106$. It should be noted that these peculiarities do not strongly depend on $\lambda_{ab}(0)$ values. This is demonstrated in the inset of Fig. 7(a), where $n_s(T)/n_0$ experimental curve for $p = 0.092$ is compared to the ones obtained using $\lambda_{ab}(0)$ increased (open stars) and decreased (solid stars) by 40 nm. Actually, the latter value is much higher than the experimental uncertainty.

The behavior of the superfluid density $n_s(T)/n_0$, as shown in Fig. 7(a), contradicts the conclusions of the precursor pairing model^{49,50} based on the formation of pair electron excitations with finite momentum at $T^* > T_c$, but agrees with the DDW scenario⁴⁵. According to⁴⁵, at temperatures much smaller than the relevant energy scales, a DDW (W_0) and DSC

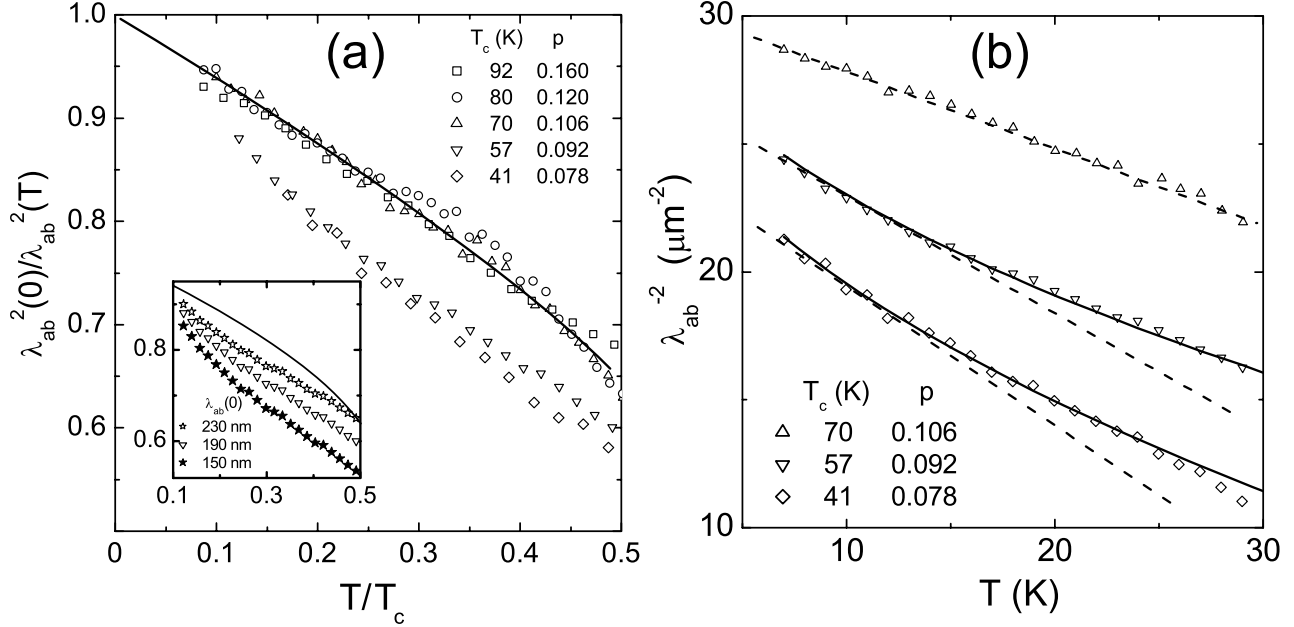


Fig. 7. (a) $\lambda_{ab}^2(0)/\lambda_{ab}^2(T) = n_s(T)/n_s(0)$ at $T < T_c/2$ in $\text{YBa}_2\text{Cu}_3\text{O}_{7-x}$ with different doping. The solid line is the $\lambda_{ab}^2(0)/\lambda_{ab}^2(T)$ dependence in BCS d -wave superconductor (DSC). The inset shows $n_s(T)/n_0$ experimental curve for $p = 0.092$ and the ones obtained using $\lambda_{ab}(0)$ increased (open stars) and decreased (solid stars) by 40 nm; (b) comparison of experimental $\lambda_{ab}^{-2}(T) \propto n_s(T)$ curves (symbols) with linear $\Delta\lambda_{ab}^{-2}(T) \propto -T$ (dashed lines) and root $\Delta\lambda_{ab}^{-2}(T) \propto -\sqrt{T}$ (solid lines) dependences for moderately doped ($p = 0.106, x = 0.33$) and heavily underdoped ($p = 0.092, x = 0.40$; $p = 0.078, x = 0.47$) $\text{YBa}_2\text{Cu}_3\text{O}_{7-x}$.

(Δ_0) order parameters at $T = 0$, only the nodal regions close to the points $(\pi/2, \pi/2)$ and symmetry-related points on the Fermi surface will contribute to the suppression of the superfluid density. In a wide range of temperatures, $n_s(T)$ dependence will be linear for the optimally and moderately doped samples, in which Δ_0 is larger than or comparable to W_0 (Fig. 8) and plays a leading role in the temperature dependence of the superfluid density. However, for the heavily underdoped samples, the situation is quite different. As the DDW gap is much larger than the superconducting gap in these heavily underdoped samples, W_0 becomes dominant around the nodes. Though in the asymptotically low-temperature regime the suppression of the superfluid density is linear on temperature, there is an intermediate temperature range over which the suppression actually behaves as \sqrt{T} . It is worth emphasizing that the authors of⁴⁵ state that these features are independent of the precise $W_0(p)$ and $\Delta_0(p)$ functional forms. The only input that is needed is the existence of DDW order, which diminishes with increase in p and complementary development of the DSC order. The DDW order eats away part of the superfluid density from an otherwise pure

DSC system. Actually, in the intermediate temperature range $0.1 T_c < T \lesssim 0.5 T_c$, the experimental $n_s(T)$ curves in $\text{YBa}_2\text{Cu}_3\text{O}_{6.60}$ and $\text{YBa}_2\text{Cu}_3\text{O}_{6.53}$ with $p < 0.1$ are not linear but similar to \sqrt{T} -dependences. This is confirmed by Fig. 7(b), where the measured curves $\lambda_{ab}^{-2}(T) \propto n_s(T)$ are compared to the linear ($\propto T$) dependences in $\text{YBa}_2\text{Cu}_3\text{O}_{6.67}$ ($p = 0.106$) and \sqrt{T} -dependences $\Delta\lambda_{ab}^{-2}(T) = -3\sqrt{T}$ (λ_{ab} and T are expressed in μm and K) in $\text{YBa}_2\text{Cu}_3\text{O}_{6.60}$ ($p = 0.092$) and $\Delta\lambda_{ab}^{-2}(T) = -3.5\sqrt{T}$ in $\text{YBa}_2\text{Cu}_3\text{O}_{6.53}$ ($p = 0.078$). Dashed lines in Fig. 7(b) correspond to the linear dependences of $\lambda_{ab}(T)$ at $T < T_c/3$, as shown in Fig. 4, and extended to higher temperatures.

It is also interesting to note that these deviations of $\Delta\lambda_{ab}^{-2}(T)$ in $\text{YBa}_2\text{Cu}_3\text{O}_{6.60}$ and $\text{YBa}_2\text{Cu}_3\text{O}_{6.53}$ are accompanied by inflection of the resistivity $\rho_{ab}(T)$ curves in the normal state of these samples. These inflections are seen at two lower $\rho_{ab}(T)$ curves in Fig. 2 around $T \sim 100$ K. Furthermore, the evolution of the temperature dependences of $\rho_c(T)$ with doping in Fig. 2 correlates with those of the c -axis penetration depth $\lambda_c(T)$. Solid symbols of Fig. 9(a) show the dependences $\lambda_c^2(0)/\lambda_c^2(T)$ at $T \leq T_c/2$ for $\text{YBa}_2\text{Cu}_3\text{O}_{7-x}$ states with $T_c = 92$, $T_c = 70$, and $T_c = 41$ K. Table I

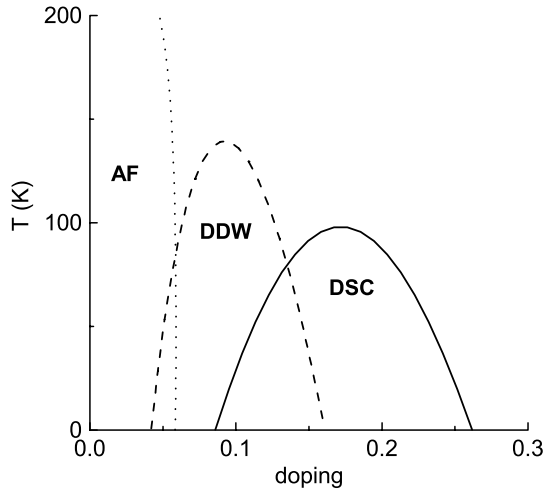


Fig. 8. The temperature versus doping p schematic phase diagram based on calculations of⁵¹. AF is the 3D antiferromagnetic phase. The system is an insulator in the AF state, a metal in the DDW and DDW + AF states, and a superconductor in the DSC and DDW + DSC states⁵¹.

contains the values of the penetration depth $\lambda_c(0)$ at $T = 0$ and the exponents α in the measured $\lambda_c(T) - \lambda_c(0) = \Delta\lambda_c(T) \propto T^\alpha$ dependences at $T \leq T_c/3$. The peculiarity of the optimally doped $\text{YBa}_2\text{Cu}_3\text{O}_{6.93}$ is

good coincidence of $\lambda_{ab}^2(0)/\lambda_{ab}^2(T)$ (open circles in Fig. 9(a) and $\lambda_c^2(0)/\lambda_c^2(T)$ temperature dependences. With the decrease of p , the temperature dependence of $\lambda_c^2(0)/\lambda_c^2(T)$ becomes substantially weaker than that of $\lambda_{ab}^2(0)/\lambda_{ab}^2(T)$. Model⁵² associates the reduction in the low- T slope of $\lambda_c^2(0)/\lambda_c^2(T)$ curves and the appearance of semiconducting-like temperature dependence of $\rho_c(T)$ with a decrease of the interlayer coupling in the crystal. Dashed line in Fig. 9(a) represents numerical result⁵² for this case. On the other hand, in the optimally doped $\text{YBa}_2\text{Cu}_3\text{O}_{6.93}$, the interlayer coupling is strong and quasiparticle transport along the c -axis becomes identical to one in the anisotropic 3D superconductor⁶. Solid line in Fig. 9(a) is $\lambda_c^2(0)/\lambda_c^2(T)$ dependence, calculated in⁵² for this particular case. So, the low- T dependences of $\lambda_c(T)$ are well-described without taking pseudogap effects into consideration. Let us consider now their possible manifestations in the doping dependence of the c -axis penetration depth.

From the inset of Fig. 9(a), it follows that reciprocal value of the zero-temperature penetration depth $1/\lambda_c(0, p)$ is roughly linear on p . Note that it vanishes at $p \approx 0.07$, which is near the value where T_c does too^{46,51}. There are several theoretical models^{52,53} and experimental confirmations⁵⁴ of the

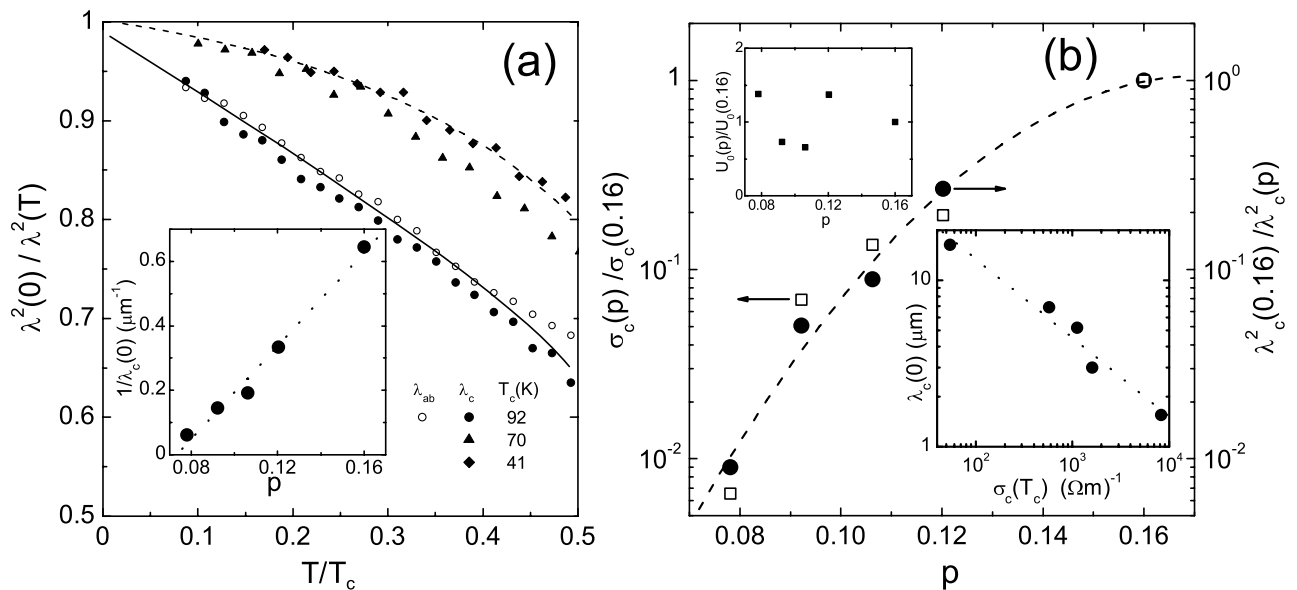


Fig. 9. (a) dependence $\lambda_{ab}^2(0)/\lambda_{ab}^2(T)$ (open symbols) in $\text{YBa}_2\text{Cu}_3\text{O}_{6.93}$ and $\lambda_c^2(0)/\lambda_c^2(T)$ (full symbols) measured for three states of the $\text{YBa}_2\text{Cu}_3\text{O}_{7-x}$ crystal with $T_c = 92$ K, $T_c = 70$ K and $T_c = 41$ K. Solid and dashed lines stand for the dependences $\lambda_c^2(0)/\lambda_c^2(T)$ calculated in⁵² for $\text{YBa}_2\text{Cu}_3\text{O}_{7-x}$ with different oxygen deficiency. The inset shows $1/\lambda_c$ at $T = 0$ as a function of doping p ; (b) doping dependences of $\lambda_c^2(p)/\lambda_c^2(0.16)$ at $T = 0$ and $\sigma_c(p)/\sigma_c(0.16)$ at $T = T_c$. Their ratio $U_0(p)/U_0(0.16)$ is shown in the upper inset. The lower inset is $\lambda_c(0)$ versus $\sigma_c(T_c)$ plot.

direct proportionality of $\lambda_c^{-2}(0)$ to the c -axis conductivity $\sigma_c(T_c)$ in HTSC. In the simplest theory, this correlation is caused by $\lambda_c^{-2} \propto J_c$ relation, where J_c is the c -axis critical current in the d -wave superconductor with anisotropic interlayer scattering and weak interlayer coupling. The value of $J_c(0)$ is determined by both the superconducting gap Δ_0 and conductivity $\sigma_c(T_c)$. The symbols in the lower inset of Fig. 9(b) show our data fitted by the dashed line $\log \lambda_c(0)[\mu m] = -0.5 \log \sigma_c(T_c)[\Omega^{-1}m^{-1}] + 2.1$. The latter constant defines a proportionality factor $U_0(p)$ in $\lambda_c^{-2}(0, p) = U_0(p) \sigma_c(T_c, p)$ relation. In the framework of DDW model, the value of $U_0(p)$ is determined by the doping dependences of $\Delta_0(p)$, $W_0(p)$ and chemical potential $\mu(p)$. As shown in⁵⁵, the opening of DDW gap can lead to increase as well as to decrease of $U_0(p)$. This depends on the position of the Fermi surface with respect to DDW gap, but in any case $U_0(p)$ changes less than twice in the whole range of doping. The values of $\lambda_c^2(0.16)/\lambda_c^2(p)$ at $T = 0$ and $\sigma_c(p)/\sigma_c(0.16)$ at $T = T_c$ are shown in Fig. 9(b). Their ratio $U_0(p)/U_0(0.16)$ is demonstrated in the upper inset of Fig. 9(b). This weak doping dependence indicates that strong decrease of the interlayer coupling integral $t_{\perp}(p) \propto \sigma_c(T_c, p)$ with lowering p ⁵⁶ in $YBa_2Cu_3O_{7-x}$ dominates over effects of the DDW order on $\lambda_c(0, p)$ ⁵⁵.

6. CONCLUSION

This paper attempts to review the main results and unsolved problems of microwave investigations of HTSC single crystals. Measurements of the surface impedance and complex conductivity of the ab -plane of the crystals with different chemical compositions are well-described in terms of the phenomenological modified two-fluid model. It seems quite natural that a consistent microscopic theory of HTSC should include the aspects of the model discussed. Namely, the theory can be based on the Fermi-liquid approach accounting for three essential factors: (i) strong electron-phonon coupling in the cuprate planes providing high- T_c values ($T_c \sim 100$ K), the linear temperature dependence of the resistivity $\Delta\rho_{ab}(T) \propto 1/\tau_{ab}(T) \propto T$ at $T > T_c$, and a broad peak in the real part of conductivity $\sigma'_{ab}(T)$ at $T < T_c$; (ii) predominant d -wave component of the superconducting order parameter leading to the linear low-temperature dependence of the penetration depth $\Delta\lambda_{ab}(T) \propto T$; (iii) layered structure and pronounced anisotropy of HTSC.

As for the underdoped states of HTSC, this wide band of HTSC phase diagram is far less investigated. Four main experimental observations of this paper viz., (i) linear dependence of $n_0(p)$ in the range $0.078 \leq p \leq 0.16$, (ii) drastic increase of low-temperature $n_s(T)$ slope at $p < 0.1$, (iii) the deviation of $\Delta n_s(T)$ dependence from universal BCS behavior $\Delta n_s(T) \propto (-T)$ at $T < T_c/2$ toward $\Delta n_s(T) \propto (-\sqrt{T})$ with decreasing $p < 0.1$, and (iv) very weak influence of pseudogap on the low- T and doping dependences of the c -axis penetration depth evidence the DDW scenario of electronic processes in underdoped HTSC.

ACKNOWLEDGMENTS

This research was supported by RFBR Grants numbers 03-02-16812, 02-02-08004 and 04-02-17358. Yu. A. N. thanks Russian Science Support Foundation.

REFERENCES

1. J. L. Tallon, C. Bernhard, H. Shaked, R. L. Hitterman, and J. D. Jorgensen, *Phys. Rev. B* **51**, 12911 (1995).
2. J. Mao, D. H. Wu, J. L. Peng, R. L. Greene, and S. M. Anlage, *Phys. Rev. B* **51**, 3316 (1995).
3. H. Srikanth, Z. Zhai, S. Sridhar, and A. Erb, *J. Phys. Chem. Solids* **59**, 2105 (1998).
4. Y. A. Nefyodov, M. R. Trunin, A. A. Zhohov, I. G. Naumenko, G. A. Emel'chenko, D. Yu. Vodolazov, and I. L. Maksimov, *Phys. Rev. B* **67**, 144504 (2003).
5. A. Hosseini, S. Kamal, D. A. Bonn, R. Liang, and W. N. Hardy, *Phys. Rev. Lett.* **81**, 1298 (1998).
6. T. Xiang, C. Panagopoulos, and J. R. Cooper, *Int. J. Mod. Phys. B* **12**, 1007 (1998).
7. S. Sridhar and W. L. Kennedy, *Rev. Sci. Instrum.* **54**, 531 (1988); M. R. Trunin, *J. Supercond.* **11**, 381 (1998).
8. M. R. Trunin and Yu. A. Nefyodov, *JETP Lett.* **77**(10), 592 (2003), cond-mat/0306158.
9. A. F. Ho and A. J. Schofield, cond-mat/0211675.
10. T. Holstein, *Ann. Phys.* **8**, 343 (1959).
11. M. R. Trunin, A. A. Zhukov, G. E. Tsydynzhapov, A. T. Sokolov, L. A. Klinkova, and N. V. Barkovskii, *JETP Lett.* **64**, 832 (1996).
12. T. Shibauchi, A. Maeda, H. Kitano, T. Honda, and K. Uchinokura, *Phys. C* **203**, 315 (1992).
13. D. Achir, M. Poirier, D. A. Bonn, R. Liang, and W. N. Hardy, *Phys. Rev. B* **48**, 13184 (1993).
14. H. Kitano, T. Shibauchi, K. Uchinokura, A. Maeda, H. Asaoka, and H. Takei, *Phys. Rev. B* **51**, 1401 (1995).
15. T. Shibauchi, H. Kitano, A. Maeda, H. Asaoka, H. Takei, I. Shigaki, T. Kimura, K. Kishio, K. Izumi, T. Suzuki, and K. Uchinokura, *J. Phys. Soc. Jpn.* **65**, 3266 (1996).

16. M. R. Trunin, A. A. Zhukov, G. A. Emel'chenko, and I. G. Naumenko, *JETP Lett.* **65**, 938 (1997).
17. M. R. Trunin and A. A. Golubov, in *Spectroscopy of High- T_c Superconductors. A Theoretical View*, N. M. Plakida, ed. (Taylor and Francis, New York, 2003) pp. 159–233.
18. T. Jacobs, S. Sridhar, Q. Li, G. D. Gu, and N. Koshizuka, *Phys. Rev. Lett.* **75**, 4516 (1995).
19. D. V. Shovkun, M. R. Trunin, A. A. Zhukov, Yu. A. Nefyodov, H. Enriquez, N. Bontemps, A. Buzdin, M. Daumens, and T. Tamegai, *JETP. Lett.* **71**, 92 (2000).
20. T. Shibauchi, H. Kitano, K. Uchinokura, A. Maeda, T. Kimura, and K. Kishio, *Phys. Rev. Lett.* **72**, 2263 (1994).
21. J. R. Waldram, D. M. Broun, D. C. Morgan, R. Ormeno, and A. Porch, *Phys. Rev. B* **59**, 1528 (1999).
22. C. Kusko, Z. Zhai, N. Hakim, R. S. Markiewicz, S. Sridhar, D. Colson, V. Viallet-Guillen, Yu. A. Nefyodov, M. R. Trunin, N. N. Kolesnikov, A. Maignan, and A. Erb, *Phys. Rev. B* **65**, 132501 (2002).
23. Yu. N. Ovchinnikov and V. Z. Kresin, *Phys. Rev. B* **65**, 214507 (2002).
24. F. F. Mende and A. A. Spitsyn, *Surface Impedance of Superconductors* (Naukova dumka, Kiev, 1985).
25. Y. A. Nefyodov, Ph.D. Thesis, Institute of Solid State Physics, 142432, Chernogolovka, Russia (2003).
26. M. R. Trunin, Y. A. Nefyodov, and H. J. Fink, *JETP* **91**, 801 (2000).
27. M. Hein, T. Kaiser, and G. Müller, *Phys. Rev. B* **61**, 640 (2000).
28. T. L. Hilton and M. R. Beasley, *Phys. Rev. B* **39**, 9042 (1989).
29. A. M. Portis and D. W. Cooke, *Supercond. Sci. Technol.* **5**, S395 (1992).
30. J. Halbritter, *J. Appl. Phys.* **68**, 6315 (1990); **71**, 339 (1992).
31. O. G. Vendik, A. B. Kozyrev, and A. Y. Popov, *Rev. Phys. Appl.* **25**, 255 (1990).
32. O. G. Vendik, L. Kowalevicz, A. P. Mitrofanov, O. V. Pakhomov, A. Y. Popov, and T. B. Samoilova, *Superconductivity: Physics, Chemistry, Technique* **3**, 1573 (1990).
33. T. Timusk and B. Statt, *Rep. Prog. Phys.* **62**, 61 (1999).
34. J. L. Tallon and J. W. Loram, *Physica C* **349**, 53 (2001).
35. M. V. Sadovskii, *Phys. Usp.* **44**, 515 (2001).
36. M. R. Norman and C. Pépin, *Rep. Prog. Phys.* **66**, 1547 (2003).
37. M. R. Trunin, Yu. A. Nefyodov, and A. F. Shevchun, *Phys. Rev. Lett.* **92**, 067006 (2004).
38. J. W. Loram, J. Luo, J. R. Cooper, W. Y. Liang, and J. L. Tallon, *J. Phys. Chem. Solids* **62**, 59 (2001).
39. C. Bernhard, J. L. Tallon, T. Blasius, A. Golnik, and C. Niedermayer, *Phys. Rev. Lett.* **86**, 1614 (2001).
40. Y. J. Uemura, *Physica C* **282–287**, 194 (1997).
41. P. A. Lee and X.-G. Wen, *Phys. Rev. Lett.* **78**, 4111 (1997).
42. A. J. Millis, S. M. Girvin, L. B. Ioffe, and A. I. Larkin, *J. Phys. Chem. Solids* **59**, 1742 (1998).
43. L. B. Ioffe and A. J. Millis, *J. Phys. Chem. Solids* **63**, 2259 (2002).
44. S. Chakravarty, R. B. Laughlin, D. K. Morr, and C. Nayak, *Phys. Rev. B* **63**, 094503 (2001).
45. S. Tewari, H.-Y. Kee, C. Nayak, and S. Chakravarty, *Phys. Rev. B* **64**, 224516 (2001).
46. Q.-H. Wang, J. H. Han, and D.-H. Lee, *Phys. Rev. Lett.* **87**, 077004 (2001).
47. D. A. Bonn, S. Kamal, A. Bonakdarpour, R. X. Liang, W. N. Hardy, C. C. Homes, D. N. Basov, and T. Timusk, *Czech. J. Phys.* **46**, 3195 (1996).
48. C. Panagopoulos, J. R. Cooper, and T. Xiang, *Phys. Rev. B* **57**, 13422 (1998).
49. I. Kostzin, Q. Chen, Y.-J. Kao, and K. Levin, *Phys. Rev. B* **61**, 11662 (2001).
50. J. Stajic, A. Iyengar, K. Levin, B. R. Boyce, and T. R. Lemberger, *Phys. Rev. B* **68**, 24520 (2003).
51. C. Nayak and E. Pivovarov, *Phys. Rev. B* **66**, 064508 (2002).
52. R. J. Radtke, V. N. Kostur, and K. Levin, *Phys. Rev. B* **53**, R522 (1996).
53. P. J. Hirschfeld, S. M. Quinlan, and D. J. Scalapino, *Phys. Rev. B* **55**, 12742 (1997); S. Chakravarty, H.-Y. Kee, and E. Abrahams, *Phys. Rev. Lett.* **82**, 2366 (1999); Y. Ohashi, *J. Phys. Soc. Jpn.* **69**, 659 (2000).
54. D. N. Basov, T. Timusk, B. Dabrowski, and J. D. Jorgensen, *Phys. Rev. B* **50**, 3511 (1994); J. R. Kirtley, K. A. Moler, G. Villard, and A. Maignan, *Phys. Rev. Lett.* **81**, 2140 (1998); S. V. Dordevic, E. J. Singley, D. N. Basov, S. Komiya, Y. Ando, E. Bucher, C. C. Homes, and M. Strongin, *Phys. Rev. B* **65**, 134511 (2002).
55. W. Kim, J.-X. Zhu, J. P. Carbotte, and C. S. Ting, *Phys. Rev. B* **65**, 064502 (2002).
56. P. Nyhus, M. A. Karlow, S. L. Cooper, B. W. Veal, and A. P. Paulikas, *Phys. Rev. B* **50**, 13898 (1994).